Journal of Solid Mechanics Vol. 8, No. 2 (2016) pp. 372-383

Creep Evolution Analysis of Composite Cylinder Made of Polypropylene Reinforced by Functionally Graded MWCNTs

A. Loghman *, H. Shayestemoghadam , E. Loghman

Department of Solid Mechanics, Faculty of Mechanical Engineering, University of Kashan, Kashan, Iran

Received 8 March 2016; accepted 6 May 2016

ABSTRACT

Polypropylene is one of the most common, fastest growing and versatile thermoplastics currently used to produce tanks and chemical piping systems. Even at room temperature creep is considerable for polypropylene products. The creep behavior of strains, stresses, and displacement rates is investigated in a thick-walled cylinder made of polypropylene reinforced by functionally graded (FG) multi-walled carbon nanotubes (MWCNTs) using Burgers viscoelastic creep model. The mechanical properties of the composite are obtained based on the volume content of the MWCNTs. Loading is composed of an internal pressure and a uniform temperature field. Using equations of equilibrium, stress-strain and strain-displacement, a constitutive differential equation containing total creep strains is obtained. Creep strain increments are accumulated incrementally during the life of the vessel. Creep strain increments are related to the current stresses and the material uniaxial Burgers creep model by the well-known Prandtl-Reuss relations. A semi-analytical solution using Prandtl-Reuss relation has been developed to determine history of stresses, strains and displacements. The results are plotted against dimensionless radius for different volume content of MWCNTs. It has been found that the creep radial and circumferential strains of the cylinder reduce with increasing content of carbon nanotubes. It has also been concluded that the uniform distribution of MWCNTs reinforcement does not considerably influence on stresses.

Keywords : Composite FG cylinder; Time-dependent creep; Burgers model; Polypropylene ;MWCNTs reinforcement CNT.

1 INTRODUCTION

POLYPROPYLENE is the lightest weight piping material with very good chemical resistance, even to many organic solvents. It is used extensively for HVAC (heating, ventilation, and air conditioning) applications. Typical applications include chemical drainage systems, industrial process, high purity water, hot and cold water distribution. Polymer based composites reinforced by carbon nanotubes have shown excellent strength properties and are recently used in the manufacture of components exposed to high pressure. Even at room temperature creep is significant for polypropylene tubes. Therefore creep analysis and creep life assessment of such vessels with cylindrical geometry are very important. Creep analysis under multi-axial states of stress is well developed by Boyle and Spence [1].When such components are loaded, thermo-elastic stresses are developed in the vessel at zero time. However, because of creep evolution, stresses are changing with time during the life of component which can affect

*Corresponding author. Tel.: +98 31 55912425; Fax: +98 31 55912424.
E-mail address: aloghman@kashanu.ac.ir (A. Loghman).

its long-time performance. Elastic solution of thick-walled nanocomposite cylinder has been studied by Ghorbanpour et al. [2]. Steady-State creep analysis of thick-walled orthotropic cylinders has been investigated by PAI [3] using piecewise linear model. The results indicated that the anisotropy has a significant effect on the cylinder creep behavior and the solution presented in the paper can help to predict creep rate more accurately. Large strain creep analysis of thick-walled cylinders has been carried out by Bhatnagar and Arya [4]. They used the finite-strain theory to study the creep behavior of a thick-walled cylinder subjected to large strains. Creep analysis of an internally pressurized orthotropic rotating cylinder under a steady state creep condition has also been studied by Bhatnagar et al. [5]. In this work, they presented stress and strain rate distributions. Primary creep analysis of an orthotropic thick-walled cylinder has also been presented by Bhatnagar et al. [6]. Evaluation of creep compliances of unidirectional fibre-reinforced composites has been presented by Moal and Perreux [7]. Modeling the anisotropy and creep in orthotropic aluminum–silicon carbide composite rotating disc were studied by Singh and Ray [8].Their investigation was carried out using Hill yield criterion and then they compared the results with von Misses yield criterion for the isotropic composites. The characterization of tensile creep resistance of polyamide 66 nanocomposites has been studied by Yang et al [9]. The study provided systematic experiments and general discussions on the creep resistance of polyamide 66 nanocomposites. To develop this work they applied both a viscoelastic Burgers creep model and empirical power law method of Findley. The results indicated that the simulating results from both models agreed quite well with the experimental data. Creep damage evaluation of thick-walled spheres using the theta projection concept has been described by Loghman and Shokouhi [10]. In this paper, they described a numerical model developed for the computation of creep damages in a thick-walled sphere subjected to an internal pressure and a thermal gradient. The results indicated that maximum damages are always located at the inner surface of the sphere, while the outer surface of the vessel sustains minimum damages. Creep stress redistribution has been analyzed in a thick-walled FGM Sphere using Prandtl-Reuss relation and the Norton's Law by Aleayoub and Loghman [11]. They illustrated initial thermo-elastic stresses for different material properties. Creep properties of aluminum-based composite containing multi-walled carbon nanotubes have been studied by Choi and Bae [12]. They considered constant volume content (4.5%) of MWCNTs as reinforcement. Creep and recovery of polypropylene carbon nanotube composites were studied by Yu Jia et al [13] using both Burger's model and Weibull distribution function. As a result the incorporation of nanotubes improved the recovery property remarkably. Time-dependent creep stress redistribution analysis of thick-walled functionally graded spheres using the method of successive elastic solution has been performed by Loghman et al [14]. Ignoring creep strains, they presented a closed-form solution for initial thermoelastic stresses at zero time. It has been also found that the material in-homogeneity parameter β has a substantial effect on thermoelastic stresses. The results also showed that the stresses and strains are changing with time at a decreasing rate so that there is a saturation condition beyond which not much change occurs. Actually, after 50 years the solution approaches the steady-state condition. Time-dependent thermoelastic creep of rotating disk made of Al–SiC composite has been analyzed by Loghman et al [15] using Mendelson's method of successive elastic solution. It is concluded that the uniform distribution of SiC reinforcement does not considerably influence on stresses. However, the minimum and most uniform distribution of circumferential and effective thermoelastic stresses belongs to composite disk of aluminum with 0% SiC at inner surface and 40% SiC at outer surface. Effect of particle content, size and temperature on magneto-thermo mechanical creep behavior of composite cylinders has been investigated by Loghman et al [16]. They showed that increasing particle size and operating temperature significantly increases the effective creep strain rates. A semi-analytical solution for time-dependent creep analysis of rotating cylinders made of anisotropic exponentially graded material (EGM) has been carried out by Loghman and Atabakhshian [17]. Time-dependent thermo-creep analysis of rotating FGM thick-walled cylindrical pressure vessels under heat flux has been studied by Nejad and Kashkoli [18]. An analytical shear-lag model for steady state creep analysis of a composite with short fibers was developed by Mileiko [19]. Using shear-lag theory and polynomial displacement functions, a novel analytical method has been developed by Monfared [20] for predicting steady state creep of short fiber metal-matrix composites. He showed that suitable agreements were found among his analytical method, numerical (FEM) and available published results. A semi-analytical method for predicting composite creep strain rate and quasi shear-lag formulation has been employed for prediction of partial creep debonding at the interface in steady state creep of short fiber composites under tensile axial stress by Monfared and Mondali [21]. Creep and recovery of polystyrene composites filled with graphene additives has been carried out experimentally by Tang et al. [22].

Although many theoretical and experimental study has been conducted on creep response of short fiber composites, however, the effects of different volume distribution of nano-fibers on the time-dependent creep response of thick-walled polymer based composite cylinders are not well developed in the literature. The main objectives of this paper is to present history of stresses, strains and displacements during creep evolution of polypropylene thick-walled cylinder reinforced by functionally graded MWCNTs.

2 GEOMETRY, MATERIAL PROPERTIES AND LOADING CONDITION

2.1 Geometry and loading condition

A long, thick-walled composite hollow cylinder made of polypropylene reinforced by functionally graded (FG) multi-walled carbon nanotubes (MWCNTs) with an inner radius r_i and outer radius r_o is considered (Fig. 1). The cylinder is subjected to an internal pressure P_i, an external pressure P_o and a uniform temperature field T. The following data for geometry and loading conditions are used in this paper. The radius ratio and internal pressure are given below. The outer pressure in this study is zero.

$$\frac{r_o}{r_i}=2 \qquad P_i=100MPa \tag{1}$$

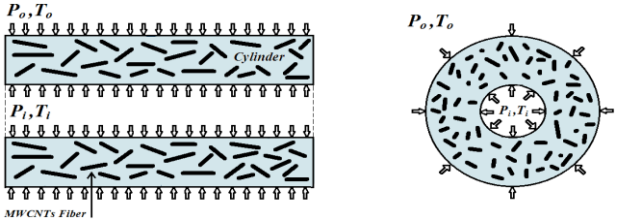

Fig.1
Geometry and loading condition of thick-walled long cylinder made of polypropylene reinforced by MWCNTs.

2.2 Material properties

Young's modulus of nanocomposite assumed to follow a linear equation which is derived from Table.1 [13].

$$E_T=a\times p+b \tag{2}$$

$$a=0.2Gpa, b=1.83Gpa \tag{3}$$

In which p is the volume percentage of MWCNT content.

Table 1
Young's modulus of propylene nanocomposite with different MWCNT contents [13].

MWCNTs content (vol.%)	Young's modulus (GPa)
0	1.83 ± 0.11
0.3	2.10 ± 0.11
0.6	2.12 ± 0.03
2.8	2.33 ± 0.14
4.5	2.42 ± 0.13

The distribution of MWCNTs fibers has been assumed to follow Eq. (4) from inner to outer surfaces of the cylinder. Thus, density and creep parameters are varying in radial direction. Three cases of volume distribution are considered for MWCNTs and shown in Fig. 2. Case (1): A uniform distribution of 3% , Case (2): a linear distribution from outer to inner surfaces and Case (3): a linear distribution from inner to outer

$$\begin{cases} case1 & P=3\% \\ case2 & P=4.5(r_o-r)/r_i \\ case3 & P=4.5(r-r_i)/r_i \end{cases} \tag{4}$$

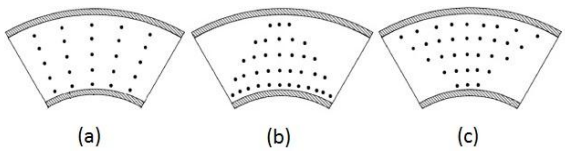

Fig.2
(a).Case 1 (b). Case 2 (c). Case3.

3 BURGERS MODEL

The creep constitutive model is the Burgers law (Eq. (5)) in which σ_0 is the initially applied stress; $\tau = \frac{\eta_k}{E_k}$ is the retardation time taken to produce 63.2% or $(1-e^{-1})$ of the total deformation in the Kelvin unit [8], η_k is the viscosity of the Kelvin spring and dashpot, respectively, η_m is the viscosity of the Maxwell spring and dashpot. Schematic diagram of Burgers model is shown in figure 3. The Burgers model, which includes the essential elements, can be applied satisfactorily to model the practical behaviors of viscoelastic materials. The material parameters, η_m, E_k, and η_k can be simulated from the experimental data. The simulated parameters of the Burger's model with different MWCNT contents for long term prediction are written in Table 2. The variation of the simulated parameters will constitutively show the effect of Nano fibers [9].

$$\dot{\varepsilon}^c = \frac{\sigma_0}{\eta_M} + \frac{\sigma_0}{\eta_K} e^{\frac{-t}{\tau}} \tag{5}$$

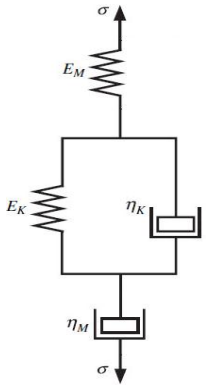

Fig.3
Schematic diagram of Burgers model [9].

Table 2
Simulated parameters of the Burger's model with different MWCNT contents for long term prediction [13].

MWCNTs (Vol.%)	E_k (MPa)	η_k (MPa s)	η_m (s)	τ (s)
0	5.7	9.00E+07	1.50E+10	1.49E+07
0.3	8.5	1.00E+08	2.10 E+10	1.53 E+07
0.6	9.2	1.50E+08	2.60 E+10	1.63 E+07
2.8	9.6	1.70E+08	2.70 E+10	1.77 E+07
4.5	10.4	2.00E+08	2.80 E+10	1.92 E+07

4 THEORETICAL ANALYSIS

Elastic solution for a thick-walled cylinder is done by A. Ghorbanpouret al [1]. Figure 1 demonstrates a thick-walled cylinder subjected to uniform internal and external pressures (P_i and P_o, respectively) and hence, cylinder deformation is axially symmetric. Furthermore, the deformations happen at a cross section sufficiently far from the junction of the cylinder and its ends, so that it is practically independent of the axial coordinate *z* as suggested by Boresi et al [23].The strain displacement relation is written as:

$$\varepsilon_r = \frac{\partial u_r}{\partial r} \tag{6}$$

$$\varepsilon_\theta = \frac{u_r}{r} \tag{7}$$

Total strains are assumed to be the sum of elastic, thermal, and creep strains. The cylinder is thick-walled and therefore, plane strain condition is considered. Moreover, cylindrical coordinate system is used and axial symmetry is assumed. For the axisymmetric plane strain problem, stress-strain relation is written in terms of total strains, and creep strains as follows:

$$\begin{bmatrix} \sigma_r \\ \sigma_\theta \end{bmatrix} = \begin{bmatrix} C_{11} & C_{12} \\ C_{12} & C_{22} \end{bmatrix} \begin{bmatrix} \varepsilon_r & \varepsilon_r^c \\ \varepsilon_\theta & \varepsilon_\theta^c \end{bmatrix} \tag{8}$$

In terms of radial displacement the above relationship can be written as follows:

$$\sigma_r = C_{11}\frac{\partial u_r}{\partial r} + C_{12}\frac{u_r}{r} - [C_{11}\varepsilon_r^c + C_{12}\varepsilon_\theta^c] \tag{9}$$

$$\sigma_\theta = C_{21}\frac{\partial u_r}{\partial r} + C_{22}\frac{u_r}{r} - [C_{21}\varepsilon_r^c + C_{22}\varepsilon_\theta^c] \tag{10}$$

$$C_{11} = \frac{E\times(1-\nu)}{(1+\nu)\times(1-2\nu)},\ C_{12} = \frac{E\times\nu}{(1+\nu)\times(1-2\nu)},\ C_{21} = C_{12},\ C_{22} = C_{11} \tag{11}$$

$$\nu = 0.45 \tag{12}$$

The value of Modulus of elasticity in Eq. (11) for each case will be determined by substituting Eq. (4) in Eq. (2).The equilibrium equation of the thick-walled composite hollow cylinder under uniform internal and external pressure is written as:

$$\frac{\partial \sigma_r}{\partial r} + \frac{\sigma_r - \sigma_\theta}{r} = 0 \tag{13}$$

Substituting Eq. (9) and Eq. (10) into equilibrium Eq. (13), the following differential equation for displacement is obtained

$$D_{11}\frac{\partial^2 u_r}{\partial r^2} + D_{12}\frac{\partial u_r}{\partial r} + D_{13}u_r + D_{14} = 0 \tag{14}$$

where

$$\begin{aligned} &D_{11} = [C_{11}],\ D_{12} = \left[\left(\frac{C_{11}}{r}\right)\right],\ D_{13} = \left[\left(\frac{-C_{22}}{r^2}\right)\right], \\ &D_{14} = -\frac{[C_{21}\varepsilon_r^c + C_{22}\varepsilon_\theta^c]}{r} + \frac{[C_{11}\varepsilon_r^c + C_{12}\varepsilon_\theta^c]}{r} + \frac{\partial[C_{11}\varepsilon_r^c + C_{12}\varepsilon_\theta^c]}{\partial r} \end{aligned} \tag{15}$$

D_{14} contains creep strains which are time, temperature and stress dependent. If we ignore time-dependent creep strains in coefficient D_{14}, then the differential Eq. (14) becomes Navier's equation. The solution of Navier's equation gives thermoelastic analysis. Thermoelastic analysis is done using the division method [24]. In this method the cylinder thickness is divided into a finite number of divisions. Then the Navier's equation for k_{th} division yields the following differential equation with constant coefficients. The Navier's equation for k_{th} division yields

$$(D_{11}^{(k)}\frac{\partial^2}{\partial r^2}+D_{12}^{(k)}\frac{\partial}{\partial r}+D_{13}^{(k)})u_r^k+D_{14}^k=0 \tag{16}$$

The coefficients of Eq. (16) are evaluated in each division in terms of constants and the radius of k_{th} division.The exact solution for Eq. (16) can be written in the form of [25]

$$u^{(k)}=X_1^{(k)}\exp(\eta_1^{(k)}r^{(k)})+X_2^{(k)}\exp(\eta_2^{(k)}r^{(k)})-\frac{D_{14}^{(k)}}{D_{13}^{(k)}} \tag{17}$$

where

$$\eta_1^{(k)},\eta_1^{(k)}=\frac{D_{12}^{(k)}\pm\sqrt{(D_{12}^{(k)})^2-4D_{13}^{(k)}D_{11}^{(k)}}}{2D_{11}^{(k)}} \tag{18}$$

It is noted that this solution for Eq. (16) is valid in the following sub-domain

$$r^{(k)}-\frac{t^{(k)}}{2}\le r\le r^{(k)}+\frac{t^{(k)}}{2} \tag{19}$$

where $t^{(k)}$ is the thickness of k_{th} division and $X_1^{(k)}$ and $X_2^{(k)}$ are unknown constants for k_{th} division. The unknowns $X_1^{(k)}$ and $X_2^{(k)}$ are determined by applying the necessary boundary conditions between two adjacent sub-domains. For this purpose, the continuity of the radial displacement u as well as radial stress σ_r is imposed at the interfaces of the adjacent sub domains. These continuity conditions at the interfaces are

$$u^{(k)}\Big|_{r=r^{(k)}+\frac{t^{(k)}}{2}}=u^{(k+1)}\Big|_{r=r^{(k+1)}-\frac{t^{(k+1)}}{2}},\qquad \sigma_r^{(k)}\Big|_{r=r^{(k)}+\frac{t^{(k)}}{2}}=\sigma_r^{(k+1)}\Big|_{r=r^{(k+1)}-\frac{t^{(k+1)}}{2}} \tag{20}$$

And global boundary conditions are

$$\sigma_r=P_i \ \ at\ \ r=r_i \qquad\qquad \sigma_r=P_o \ \ at\ \ r=r_o \tag{21}$$

The continuity conditions Eq. (20) together with the global boundary conditions Eq. (21) yield a set of linear algebraic equations in terms of $X_1^{(k)}$ and $X_2^{(k)}$. Solving the resultant linear algebraic equations for $X_1^{(k)}$ and $X_2^{(k)}$, the unknown coefficients of Eq. (17) are calculated. Then, the displacement component u_r and the stresses are determined in each radial sub-domain. Increasing the number of divisions improves the accuracy of the results.

5 TIME - DEPENDENT CREEP ANALYSIS

For time-dependent creep analysis, the creep strains in coefficient D_{14} must be considered. Creep strains are time, temperature, and stress dependent. Creep strain increments are related to the current stresses and the material uni-axial creep behavior by the well-known Prandtl–Reuss relation. For problems of thick-walled cylinder with radial symmetry, these relations are [26]

$$\begin{aligned}
\dot{\varepsilon}_r^c&=\frac{\dot{\varepsilon}_c}{2\sigma_e}[2\sigma_r-(\sigma_\theta+\sigma_z)]\\
\dot{\varepsilon}_\theta^c&=\frac{\dot{\varepsilon}_c}{2\sigma_e}[2\sigma_\theta-(\sigma_r+\sigma_z)]\\
\dot{\varepsilon}_z^c&=\frac{\dot{\varepsilon}_c}{2\sigma_e}[2\sigma_z-(\sigma_r+\sigma_\theta)]
\end{aligned} \tag{22}$$

where $\dot{\varepsilon}_r^c$, $\dot{\varepsilon}_\theta^c$ and $\dot{\varepsilon}_z^c$ are radial, circumferential, and axial creep strain rates, $\dot{\varepsilon}_c$ and σ_c are equivalent creep strain rate and equivalent stress, respectively. These equivalent or effective variables are defined as follows:

$$\begin{aligned}
&\dot{\varepsilon}_c = \frac{2}{\sqrt{3}}\sqrt{(\dot{\varepsilon}_r^c)^2 + (\dot{\varepsilon}_\theta^c)^2 + (\dot{\varepsilon}_z^c)^2} \\
&\sigma_e = \sqrt{\frac{1}{2}((\sigma_r - \sigma_\theta)^2 + (\sigma_r - \sigma_z)^2 + (\sigma_\theta - \sigma_z)^2)} \\
&\dot{\varepsilon}_z^c = 0 \rightarrow \sigma_z = 0.5(\sigma_r + \sigma_\theta)
\end{aligned} \tag{23}$$

The material creep constitutive model Eq. (5) can be rewritten in terms of equivalent creep strain rate and equivalent stress as:

$$\dot{\varepsilon}_c = \left(\frac{\sigma_0}{\eta_M} + \frac{\sigma_0}{\eta_K} e^{\frac{-t}{\tau}}\right) \tag{24}$$

Eqs. (22), (23), and (24) in conjunction with differential Eq. (16) are used in a numerical procedure based on the Mendelson's method of successive elastic solution [27] to obtain history of stresses and deformations during creep process. The results are illustrated in Figs. 4 to 19.

6 RESULTS AND DISCUSSION

The results presented in this paper are for three cases of FG distribution of MWCNTs in the matrix of polypropylene. These cases are defined and illustrated in section 2 of this paper.

Dimensionless radial displacements for the FG cylinder reinforced by MWCNTs after three and ten years are shown in Figs. 4 and 5 respectively. The dimensionless radial displacement for the case 2 is much lower than other two cases after 3 and 5 years. This is because, in case 2, the maximum 4.5% MWCNTs reinforcement is located at the inner surface of the vessel and the maximum effective stress is also located at the inner surface. It is also clear that, due to time-dependent creep deformation, radial displacement after 10 years is greater than after 3 years for all 3 cases.

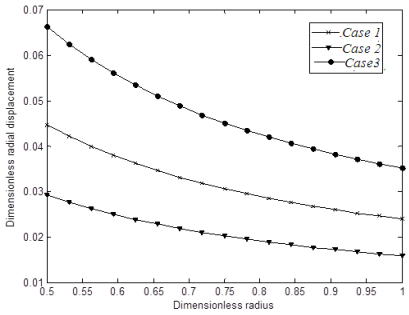

Fig.4
Dimensionless radial displacement in the FGM cylinder after 3 years for the case 1,2 and 3.

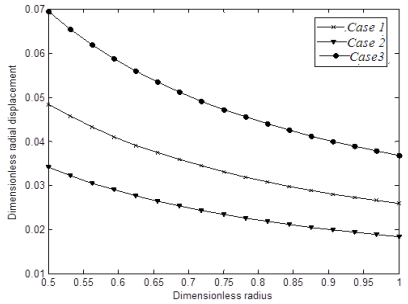

Fig.5
Dimensionless radial displacement in the FGM cylinder after 10 years for the case 1,2 and 3.

Dimensionless radial, circumferential and effective stresses after 3 and 10 years are plotted against dimensionless radius for three cases in Figs. 6 to 11. Figs. 6 and 7 show radial stresses after 3 and 10 years which satisfy the boundary condition. There are not significant differences among radial stresses for all three cases, however, the minimum absolute value belongs to case 2 and its maximum absolute value belongs to case 3. Radial stress redistribution is not really considerable and there are no significant changes in radial stresses after three and ten years. This is because of the fixed values of boundary condition for radial stresses at the inner and outer surface of the cylinder. It can also be justified comparing radial stress histories with the published literature [17, 26].

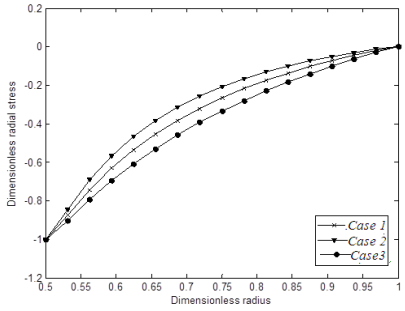

Fig.6
Dimensionless radial stress in the FGM cylinder after 3 years for the case 1,2 and 3.

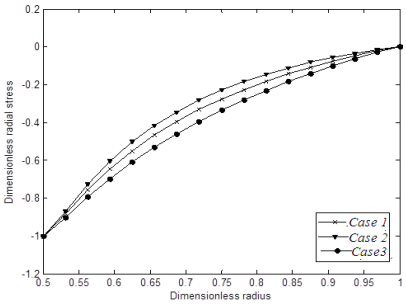

Fig.7
Dimensionless radial stress in the FGM cylinder after 10 years for the case 1,2 and 3.

Figs. 8 and 9 represent a comparison between circumferential stresses after 3 and 10 years for three cases. Circumferential stresses are decreasing with time at the inner surface of the cylinder and increasing at the outer surface of the vessel for all three cases. It is because of higher deformations of the cylinder which occurs at the inner surface and lower at the outer surface of the vessel. They are tensile throughout thickness for all three cases, however, for case 1and case 3 they are highly tensile at the inner surface of the cylinder where the radial stresses are highly compressive. It means the maximum shear stress which is $\tau_{max} = (\sigma_\theta - \sigma_r)/2$ will be very high at the inner surface of the FG cylinder. Therefore in selection of carbon nano-tube content and distribution for such a cylinder the case 2 should be selected because of the uniform shear stress distribution throughout thickness. This can be well understood from Figs. 10 and 11 in which the effective stress distribution throughout thickness is shown for all three cases of carbon nano-tube distribution. Also in Figs. 10 and 11 a reference stress point can be identified for which effective stress is independent of carbon nano-tube content and time. Such a reference stress has also been observed in [17]. It can also be observed that the best uniform effective stress distribution belongs to the case 2.

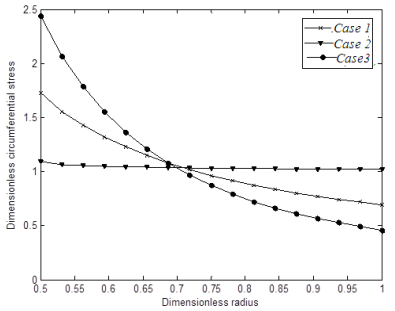

Fig.8
Dimensionless circumferential stress in the FGM cylinder after 3 years for the case 1,2 and 3.

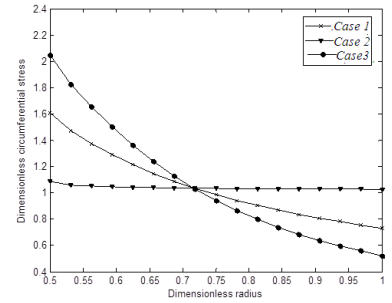

Fig.9
Dimensionless circumferential stress in the FGM cylinder after 10 years for the case 1,2 and 3.

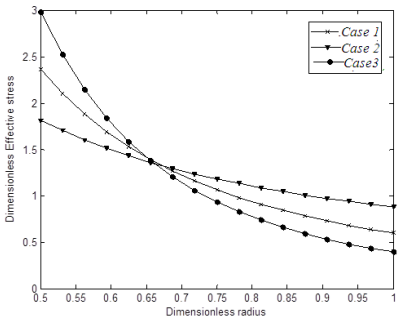

Fig.10
Dimensionless effective stress in the FGM cylinder after 3 years for the case 1,2 and 3.

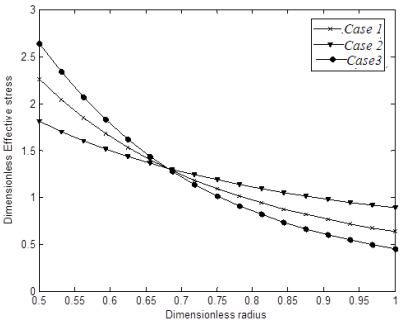

Fig.11
Dimensionless effective stress in the FGM cylinder after 10 years for the case 1,2 and 3.

Figs. 12 to 15 show radial and circumferential total strains of the composite cylinders for three cases after 3 and 10 years. The absolute values of total strains are increasing with time due to creep deformation. However because of higher deformation at the inner surface of the vessel (Figs 3 and 4) higher variation of strains can be observed in this region as expected. It is also clear that minimum absolute values of total strains belong to the case 2.

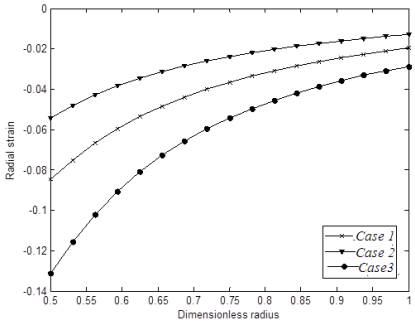

Fig.12
Radial strain in the FGM cylinder after 3 years for the case 1,2 and 3.

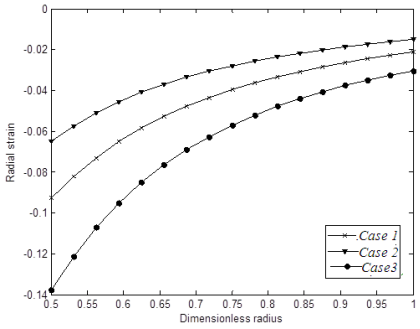

Fig.13
Radial strain in the FGM cylinder after 10 years for the case 1,2 and 3.

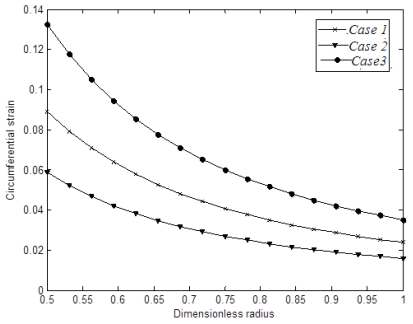

Fig.14
Circumferential strain in the FGM cylinder after 3 years for the case 1,2 and 3.

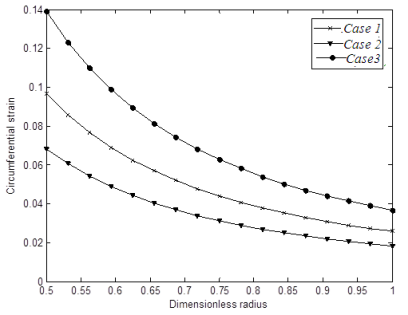

Fig.15
Circumferential strain in the FGM cylinder after 10 years for the case 1,2 and 3.

Figs. 16 to 19 represent radial and circumferential creep strain for all three cases after 3 and 10 years. Absolute values of creep strains are increasing with time due to creep deformation as expected. However these figures show that maximum absolute values of creep strains are located at the inner surface of the cylinder owing to this fact that the cylinder is exposed to internal pressure and higher deformations are located at the inner surface. Absolute values of creep strains for the case 2 are considerably less than other two cases at the inner surface of the cylinder, however there are not significant differences among them at the outer surface of the vessel. Therefore, we can come to this conclusion that case 2 is the most appropriate model for adding MWCNT short fibers to the polypropylene matrix.

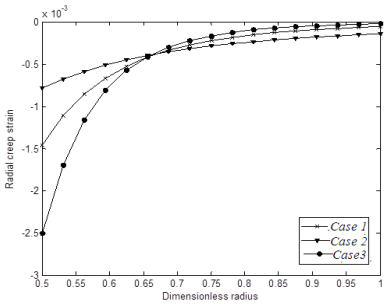

Fig.16
Radial creep strain in the FGM cylinder after 3 years for the case 1,2 and 3.

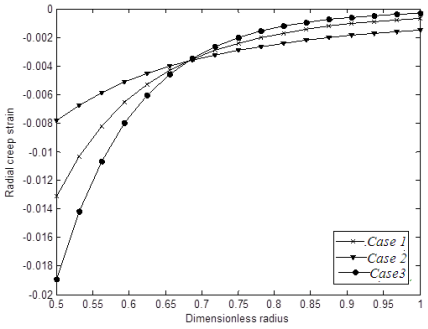

Fig.17
Radial creep strain in the FGM cylinder after 10 years for the case 1,2 and 3.

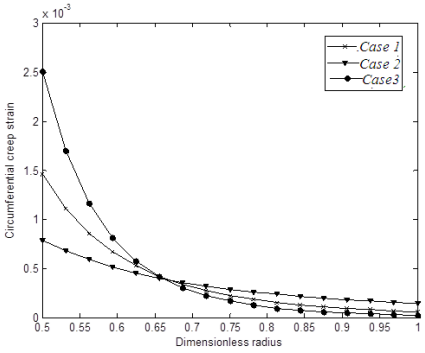

Fig.18
Circumferential creep strain in the FGM cylinder after 3 years for the case 1,2 and 3.

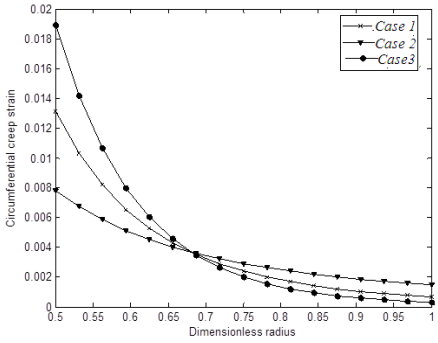

Fig.19
Circumferential creep strain in the FGM cylinder after 10 years for the case 1,2 and 3.

6 CONCLUSIONS

Time-dependent creep stress redistribution analysis of thick-walled FG cylinder made of polypropylene reinforced by MWCNTs is investigated using Burgers visco-elastic model. Three cases of FG distribution of MWCNTs in the matrix of polypropylene have been considered. It has been found that the reinforcement volume content has a substantial effect on stresses, strains and displacements. It has also been shown that radial stress redistributions are not significant, in comparison with circumferential and effective stresses. Furthermore, the maximum shear stress in case 1 and case 3 will be very high at the inner surface of the FG cylinder. Thus, in selection of material for such a cylinder the reinforcement distribution identified in case 2 should be selected because of the uniform effective and shear stress distribution throughout thickness.

ACKNOWLEDGEMENTS

The authors are grateful to University of Kashan for supporting this research.

REFERENCES

[1] Boyle J.T, Spence J.,1983, *Stress Analysis for Creep*, Butterworth-Heinemann, Southampton, Butterworth, UK.

[2] Ghorbanpour Arani A., Haghshenas A., Amir S., Mozdianfard M., Latifi M., 2013, Electro-thermo mechanical response of thick-walled piezoelectric cylinder reinforced by boron nitride nanotubes, *Strength of Materials* **45** (1): 102-115.

[3] PAI D.H., 1967, Steady-state creep analysis of thick-walled orthotropic cylinders, *International Journal of Mechanical Sciences* **9** : 335-348.

[4] Bhatnagar N.S., Arya V.K., 1974, Large strain creep analysis of thick-walled cylinders, *International Journal of Non-Linear Mechanic* **9** : 127-140.

[5] Bhatnagar N.S., Kulkarni P.S., Arya V. K., 1984, Creep analysis of an internally pressurized orthotropic rotating cylinder, *Nuclear Engineering and Design* **83** : 379-388.

[6] Bhatnagar N.S., Pradnya K., Arya V. K., 1986, Analysis of an orthotropic thick-walled cylinder under primary creep conditions, *International Journal of Pressure Vessels and Piping* **23** : 165-185.

[7] Le Moal P., Perreux D., 1994, Evaluation of creep compliances of unidirectional fibre-reinforced composites, *Composites Science and Technology* **51**: 469-477.

[8] Singh S.B., Ray S., 2002, Modeling the anisotropy and creep in orthotropic aluminum–silicon carbide composite rotating disc, *Mechanics of Materials* **34** : 363-372.

[9] Yang J.L., Zhang Z., Schlarb A.L., Friedrich K., 2006, On the characterization of tensile creep resistance of polyamide 66 nanocomposites. Part II: Modeling and prediction of long-term performance, *Polymer* **47** : 6745- 6758.

[10] Loghman A. , Shokouhi N., 2009, Creep damage evaluation of thick-walled spheres using a long-term creep constitutive model, *Journal of Mechanical Science and Technology* **23** : 2577-2582.

[11] Aleayoub S.M.A., Loghman A., 2010, Creep stress redistribution analysis of thick-walled FGM sphere, *Journal of Solid Mechanics* **2** : 115-128.

[12] Choi H.J., Bae D.H., 2011, Creep properties of aluminum-based composite containing multi-walled carbon nanotubes, *Scripta Materialia* **65** : 194-197.

[13] Jia Y., Peng K., Gong X.L., Zhang Z., 2011, Creep and recovery of polypropylene/carbon nanotube composites, *International Journal of Plasticity* **27** : 1239-1251.

[14] Loghman A., Ghorbanpour Arani A., Aleayoub S.M.A., 2011, Time-dependent creep stress redistribution analysis of thick-walled functionally graded spheres, *Mechanics of Time-Dependent Materials* **15** : 353-365.

[15] Loghman A., Ghorbanpour Arani A., Shajari A. R., Amir S., 2011, Time-dependent thermo- elastic creep analysis of rotating disk made of Al–SiC composite, *Archive of Applied Mechanics* **81** : 1853-1864.

[16] Loghman A., Askari Kashan A., Younesi Bidgoli M., Shajari A. R., Ghorbanpour Arani A., 2013, Effect of particle content, size and temperature on magneto-thermo-mechanical creep behavior of composite cylinders, *Journal of Mechanical Science and Technology* **27**: 1041-1051.

[17] Loghman A., Atabakhshian V., 2012, Semi-analytical solution for time-dependent creep analysis of rotating cylinders made of anisotropic exponentially graded material (EGM), *Journal of Solid Mechanics* **4** (3): 313-326.

[18] Nejad M. Z., Kashkoli M. D., 2014, Time-dependent thermo-creep analysis of rotating FGM thick-walled cylindrical pressure vessels under heat flux, *International Journal of Engineering Science* **82** : 222-237.

[19] Mileiko S.T., 1970, Steady state creep of a composite with short fibers, *Journal of Materials Science* **5** : 254-261.

[20] Monfared V., 2015, A displacement based model to determine the steady state creep strain rate of short fiber composites, *Composites Science and Technology* **107**: 18-28.

[21] Monfared V., Mondali M., 2014, Semi-analytically presenting the creep strain rate and quasi shear-lag model as well as FEM prediction of creep debonding in short fiber, *Composites Materials and Design* **54** : 368-374.

[22] Tang L.C., Wang X., Gong L.X., Peng K., Zhao L., Chen Q., Wu L.B., Jiang J.X., Lai G.Q., 2014, Creep and recovery of polystyrene composites filled with graphene additives, *Composites Science and Technology* **91**: 63-70.

[23] Boresi A. P., Schmidt R. J., Sidebottom O. M., 1993, *Advanced Mechanics of Materials*, John Wiley & Sons .

[24] Ghorbanpour Arani A., Loghman A., Shajari A. R., Amir S., 2010, Semi-analytical solution of magneto-thermo elastic stresses for functionally graded variable thickness rotating disks, *Journal of Mechanical Science and Technology* **24** : 2107-2117.

[25] Hosseini Kordkheili S.A., Naghdabadi R., 2007, Thermo-elastic analysis of a functionally graded rotating disk, *Composite Structures* **79** : 508-516 .

[26] Loghman A., Ghorbanpour Arani A., Amir S., Vajedi S., 2010, Magnetothermoelastic creep analysis of functionally graded cylinders, *International Journal of Pressure Vessels and Piping* **87**: 389-395.

[27] Mendelson A., 1968, *Plasticity Theory and Applications*, The Macmillan Company, New York .